A New Path Planning Algorithm Based on GNSS Localization Error Map

Guohao Zhang, Li-Ta Hsu
Interdisciplinary Division of Aeronautical and Aviation Engineering, The Hong Kong Polytechnic University

BIOGRAPHY

Mr. Guohao Zhang received the bachelor and MSc degrees in Mechanical Engineering and Automation from University of Science and Technology Beijing, China, in 2015 and in Mechanical Engineering from The Hong Kong Polytechnic University, Hong Kong in 2017, respectively. He is currently a research assistant at Interdisciplinary Division of Aeronautical and Aviation Engineering, The Hong Kong Polytechnic University. His research interests including GNSS localization, UAV navigation, sensor fusion technics and machine learning.

Dr. Li-Ta Hsu received the B.S. and Ph.D. degrees in aeronautics and astronautics from National Cheng Kung University, Taiwan, in 2007 and 2013, respectively. He is currently an assistant professor with Interdisciplinary Division of Aeronautical and Aviation Engineering, The Hong Kong Polytechnic University, before he served as post-doctoral researcher in Institute of Industrial Science at University of Tokyo, Japan. In 2012, he was a visiting scholar in University College London, U.K. His research interests include GNSS positioning in challenging environments and localization for autonomous driving vehicle and unmanned aerial vehicle.

ABSTRACT

The mission of the future parcel delivery will be performed by UAV. However, the GNSS localization in urban area usually experience the notorious multipath effect and non-line-of-sight (NLOS) reception which could potential cause about 50 meters of positioning error. This misleading localization result can be hazardous for UAV applications in the GNSS-challenged areas. However, due to the complexity of multipath, there is no general solution to eliminate the effect. A solution for guiding unmanned aerial vehicle (UAV) operation in the urban area is to plan an optimal route that smartly avoided the area with the dangerous multipath effect. To achieve this goal, the impact of multipath effect in terms of positioning error at different locations must be understood. One method is to simulate the reflection route by ray-tracing algorithm with the aids of predicted satellite positions and the widely available 3D building model. Thus, the multipath effect in pseudorange domain can be simulated using the reflection route and multipath noise envelope according a correlator design. By the reconstructing the multipath-biased pseudorange, the simulated positioning error could be obtained using least square positioning algorithm. Thus, the GNSS error distribution of a wide target area can be further constructed. With the positioning error distribution and 3D building models, an optimal path that avoided not only obstacles but also high multipath effect area can be planned. Both new A* and potential field path planning algorithms are developed to combine with the GNSS error distribution. For the former one, this paper designs a new cost function to consider both the distance to destination and the positioning error at each grid. For the potential field algorithm, a new repulsive field considered both obstacles and high positioning error is developed. By comparing the conventional and the proposed path planning algorithms, the proposed methods can plan paths with less positioning error, namely safer routes for UAV in urban areas.

1. INTRODUCTION

Unmanned Aerial Vehicles (UAV) are widely used in military and civilian applications, such as military reconnaissance, searching and rescuing for disaster [1] and future package delivering, due to its advantages of high flexibility. Recent years, the development of multi-rotor UAV provides a carrier of highly controllability and flexibility. These characteristics allow employing UAV to enable many potential civilian applications.

The operation of UAV is highly depending on its localization, which provides the accurate position of the UAV in order to navigate it correctly and safely executing the task. The most common method is using the Global Navigation Satellite System (GNSS) receiver for UAV operation. By receiving satellite signals and calculating the distance between satellite and receiver on UAV, the location of UAV is able to be determined and further aiding the navigation.

https://doi.org/10.33012/2017.15269

As UAV being more employable for civilian applications, it is required to operate in the area closer to people including urban areas. Urban area is surrounded by a great amount of buildings, which are obstacles for UAV. Operating UAV in these areas is highly restricted for the purpose of assuring safety. Hence, the precision of the localization can closely influence the performance and safety of UAV in urban area. However, the conventional localization method of GNSS is not reliable for urban application [2]. The accuracy of GNSS positioning solution will be highly affected by the satellite signal blockage and multipath effect by surrounding buildings. Since more satellite from different constellation has been launched, the total amount of satellite number could become sufficient in urban area. The major challenge for GNSS localization is still the multipath effect. It occurs when a user device receives signal reflections, resulting the aggregate signals deceive receiver tracking loop to induce an additional signal delay. Especially when the number of clean measurement is limited, the GNSS positioning result will be highly deteriorated by the multipath signal. Currently, the multipath error has no complete solution but only to mitigate such effect.

To improve the localization accuracy in urban areas, a general approach is to implement additional sensor to compensate inaccurate GNSS solutions. A popular method is to integrate inertial measurement unit (IMU) with GNSS to form a complementary integration system to obtain accurate and stable positioning performance [3]. Recent research also uses Light Detection and Ranging (LiDAR) scanner to detect the surrounding obstacles and achieve localization via Simultaneous Localization and Mapping (SLAM) technology [4]. SLAM can also improve the performance of localization in urban area [5]. Some research employs on-board vision system for SLAM to achieve localization and avoiding obstacles in the GPS-denied area [6]. These methods are able to obtain accurate localization result, but extra devices increase extra weight for UAV with limited payload. Besides, high computation loads also reduce the operation time of UAV. Those high-end sensors are too expensive for wide commercial applications, so we propose a low-cost solution rely on only GPS for UAV navigation rather than LiDAR or camera. A novel idea to ensure UAV safety will not be affected by misleading localization results in urban area is to avoid it flying in the areas with erroneous GNSS localization result, which is the objective of this paper. To achieve this goal, a new path planning algorithm is required.

For UAV path planning, there are different categories of path planning algorithm on determining the optimal path [7]. One approach is to used grid method to divide the environment into serval nodes, then calculates the cost of each step and selects the lowest cost. Thus, the shortest path to the destination can be found. This path planning method includes Dijkstra algorithm [8] and further developed to the well-known A* algorithm [9-12]. These methods are able to avoid UAV crashing on obstacles by previously knowing the obstacle locations. The A* method is applied in urban area avoiding quadcopter crushing on buildings with constructing a model of obstacles in [13]. A cost distribution map is built to guide the path determination in urban area [14]. The cost map of the environment evaluates the risk. Merging it with A* algorithm achieves planning safety path. Also, many improved path planning algorithm is developed from the A*. The planned path is further processed to be smoother considering the physical limitation of UAV turning [15]. A light assisting method is proposed to aid A* by searching less nodes [16]. The heading constraints of UAV is improved in A* for better route planning [17]. The A* is improved to design path under dynamic situation [18], and the dynamic searching speed is improved in [19, 20]. The A* category path planning method are also capable to include extra information from environment to determine the optimal path by modifying the cost function, such as the risk distribution [17] and signal strength [21, 22]. Another path planning approach is to build up artificial potential fields in the environment as attractive and repulsive fields for destination and obstacles, respectively. The path will be planned by the displacement due to overall force. This algorithm has been used to avoid obstacles with efficient and relative ideal path that more likely to operate for real-time [23]. The improvements is also developed as enabling planning path for multi-UAV avoiding static and dynamic obstacles [29], improving controllability for complex environment as [24] and cooperating with sensor detection for real-time indoor operation [25]. Other path planning category such as the genetic algorithm (GA) [26] is developed based on the genetic characteristic to determine optimal path. Other algorithms are developed by the principle of machine learning [27] or decision process with real-time uncertainty calculation [28]. Performance analysis and review of the various path planning methods can be found at [29]. Comparing with these methods, the A* algorithm selects for a global optimal path to avoid local optimal problem. It is usually applied for offline planning due to its highly computation load. The potential field can achieve faster calculation with acceptable path which can be more applied for on-board planning. For the GA method, its convergence to an ideal solution may not be guaranteed in some cases [30].

In this study, we analyze the GNSS positioning error by a multipath signal simulation model [31] and further obtain the positioning error distribution of the operating area. By predicting the satellites' position through almanac data and simulating signal reflection paths by 3D building model and ray-tracing technique, the multipath effect and none-line-of-sight (NLOS) reception can be modelled. After processing the predicted line-of-sight (LOS) and the multipath signals of a specified location, its positioning error can be also predicted. By processing all locations within the target area, the positioning error distribution can be generated. Due to the error distribution is based on prediction, an offline planning method is preferred. We hence propose a new A* algorithm. This new A* algorithm takes advantage of the predicted error distribution. The positioning error on each node is used as additional factor in the cost function. It means the higher positioning error denotes the larger traveling cost. By considering the positioning error, the UAV is able to find a path between start point and destination that avoided the obstacles (building in urban areas) and hazardous GPS-biased area at the same time. By comparing the result with conventional

A* algorithm and conventional potential field method, the proposed A* path planning can plan a path that experienced less unexpected GPS error. Namely, a path that is safer with relatively short traveling distance for UAV.

This paper is consisted of 5 sections. In section II, the GNSS positioning error in urban area of Hong Kong is analyzed with simulation, in addition, the generation of positioning error map is introduced. In section III, the detail of the improved A* path planning algorithm based on positioning error is presented. The conventional A* method and potential field method are also briefed introduced. In section IV, the verification and of multipath simulation model is shown. The result of the proposed path planning algorithm is evaluated. Finally, conclusions are drawn in section V.

2. Multipath and NLOS Modelling

Low-cost UAV relies on the GPS position solution to avoid crashing on obstacles. The GPS performance is affected by the measurement errors, including satellite clock/orbit bias, atmospheric delays, receiver thermal noise and multipath delays. The measurement errors are originated from time delays due to the effect of the error sources mentioned above. The equation is as following:

$$\delta t_D = \delta t_{atm} + \delta t_{noise} + \delta t_{mp} + \delta t_{sat} \tag{1}$$

The overall time offset δt_D is the summation of different delays, including the atmosphere errors δt_{atm}, the receiver thermal noise δt_{noise}, multipath offset δt_{mp} and satellite clock and orbit bias δt_{sat}. There are several models to mitigate or eliminate the errors above. The atmospheric delay is caused from the signal transporting through the ionosphere and troposphere layers, where the satellite signals are influenced by free electrons and free-propagation effects. Fortunately, these errors can be eliminated by differential GPS technique (DGPS). In general, the receiver thermal noise in current device is less than the order of a decimeter, which is negligible compared to other errors. The multipath error is caused by receiving the reflected signals. Due to the extra traveling distance from reflection, the signal experience a transporting time error which further influence the accuracy of the pseudorange measurement. The multipath effect is highly depending on the surrounding environment, hence DGPS cannot mitigate it. There are several methods to coarsely mitigate multipath effects, such as sophisticated discriminator design and hardware enhanced antennas. However, there is still no complete solution to eliminate this effect. When the UAV operation area is settled in urban area with many high buildings surrounding, the multipath effect will be very severe, resulting it becomes the dominant factor for GPS positioning accuracy. In this study, we focus on the positioning error introduced by multipath effect. The first goal of this paper is to construct a predicted GPS positioning error in a target area. To do this, we applied a previously developed multipath model based on 3D building model and ray-tracing simulation [31]. They are used to track the signal transmission path through direct and reflection path. The multipath model is briefly introduced as following. The position of satellite can be predicted by the broadcast almanac. Given the satellite and a receiver location, the direct signal transmission path can be easily determined. The reflection path is simulated by ray-tracking technique. We assume that reflection follows the law of reflection. If we can find a valid reflection point on 3D building model, then the reflection path can be simulated. If there are multiple reflection paths can be found for a single satellite, the path with shortest transporting distance is regarded as the main multipath effect.

This paper not only simulates the multipath but also NLOS effects. For the NLOS, its simulation is relatively simple. It is modelled as the reflection path $R_n^{refl(i)}$ subtracts the direct path $R_n^{(i)}$ as below:

$$\varepsilon_n^{\mathrm{refl}(i)} = R_{\mathrm{n}}^{\mathrm{refl(i)}} - R_n^{(i)} \ , \varepsilon_n^{refl(i)} \in NLOS \tag{2}$$

where the superscript $^{(i)}$ denotes the index of satellite and the subscript $_n$ denotes a specific location. With regards to the multipath effect, its effect on pseudorange domain is also determined by the design of correlator in receiver code tracking loop. Different correlator behaviors differently in terms of multipath noise envelope [32]. This paper selects a strobe correlator [33] to model its noise envelope *NE*, which is modelled based on correlator spacing and the relative signal strength of reflection comparing to LOS. Heuristically, we assume the multipath effect is about 6dB weaker than the LOS signal, and the spacing of the strobe correlator is 0.2 chip. Thus, multipath can be modelled as below.

$$\varepsilon_n^{\mathrm{refl}(i)} = NE\left(R_{\mathrm{n}}^{\mathrm{refl(i)}} - R_n^{(i)}\right), \varepsilon_n^{refl(i)} \in Multipath \tag{3}$$

Comparing (2) and (3), the NLOS is solely based on the additional travelling distance. Thus, it would induce larger positioning error comparing to multipath. By means of the strobe correlator, the multipath with large reflecting distance will only induce little pseudorange error [32].

The 3D building model used is constructed via Google Earth. We create the outline of the building to fit in the location on the map. After constructing the outlines, the outlines are stretched as the same height with the building. For complicated building structures with different outlines along its height, the building is separated to different polygons. The simulating area is selected in an urban area in Kowloon, Hong Kong, which is demonstrated in Fig.1.

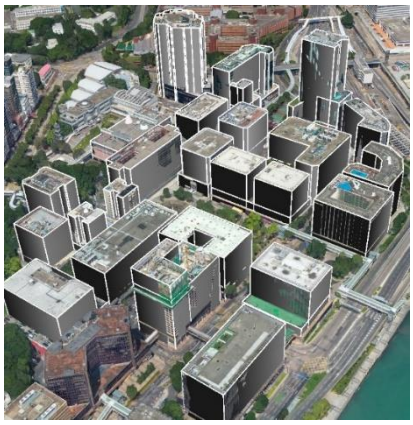

Fig.1 Constructed 3-dimensional building model.

Focusing on the multipath effect on positioning error and neglecting other errors, the simulated pseudorange is given as:

$$\rho_n^{(i)} = R_n^{(i)} + \varepsilon_n^{refl(i)} \tag{4}$$

$\rho_n^{(i)}$ is the predicted pseudorange as the summation of geometric distance $R_n^{(i)}$, which determined via the ground reference location $\mathrm{P}_n^{(i)}$ and the satellite position $\mathrm{X}_n^{(i)}$ and the multipath signal delay distance $\varepsilon_n^{\mathrm{refl}(i)}$. After simulating all the available satellite, the pseudorange can be used to calculate the predicted GPS positioning result. In this study, we assume the user device clock and the satellite clocks are perfectly synchronized, hence the positioning calculation is given as:

$$\Delta\rho_n^{(i)} = \hat{\rho}_n^{(i)} - \rho_n^{(i)} \tag{5}$$

$$\Delta \mathrm{x}^{(\mathrm{i})} = (\mathrm{H}^{(\mathrm{i})^{\mathrm{T}}}\mathrm{H}^{(\mathrm{i})})^{-1}\mathrm{H}^{(\mathrm{i})^{\mathrm{T}}}\Delta\rho^{(\mathrm{i})} \tag{6}$$

$$\mathrm{x}^{(\mathrm{i})} = \hat{\mathrm{x}}^{(\mathrm{i})} + \Delta \mathrm{x}^{(\mathrm{i})} \tag{7}$$

Assuming the approximate receiver position location as $\hat{\mathrm{x}}^{(\mathrm{i})}$ with an unknown difference $\Delta \mathrm{x}^{(\mathrm{i})}$ to the actual location. For the n^{th} satellite, $\hat{\rho}_n^{(i)}$ denotes the geometric distance between the approximate location and the n^{th} satellite. $\rho_n^{(i)}$ denotes the predicted pseudorange. The pseudorange difference $\Delta\rho_n^{(i)}$ can be calculated. With the direction cosine matrix of pseudorange $\mathrm{H}^{(\mathrm{i})}$ and the pseudorange differences, the difference $\Delta \mathrm{x}^{(\mathrm{i})}$ can be solved via iterative least square method. The predicted positioning solution $\mathrm{x}^{(\mathrm{i})}$ can be determined by correcting the approximate location with $\Delta \mathrm{x}^{(\mathrm{i})}$. After obtaining $\mathrm{x}^{(\mathrm{i})}$ for the i^{th} location, the positioning error $\varepsilon_{pe}^{(i)}$ due to multipath effect can be calculated by comparing with the real i^{th} location $\mathrm{x}_{real}^{(i)}$ as follows:

$$\varepsilon_{pe}^{(i)} = \left\| \mathrm{x}^{(\mathrm{i})} - \mathrm{x}_{real}^{(i)} \right\| \tag{8}$$

Repeating the process for all the locations in the target area, the distribution of the predicted positioning error can be finally obtained.

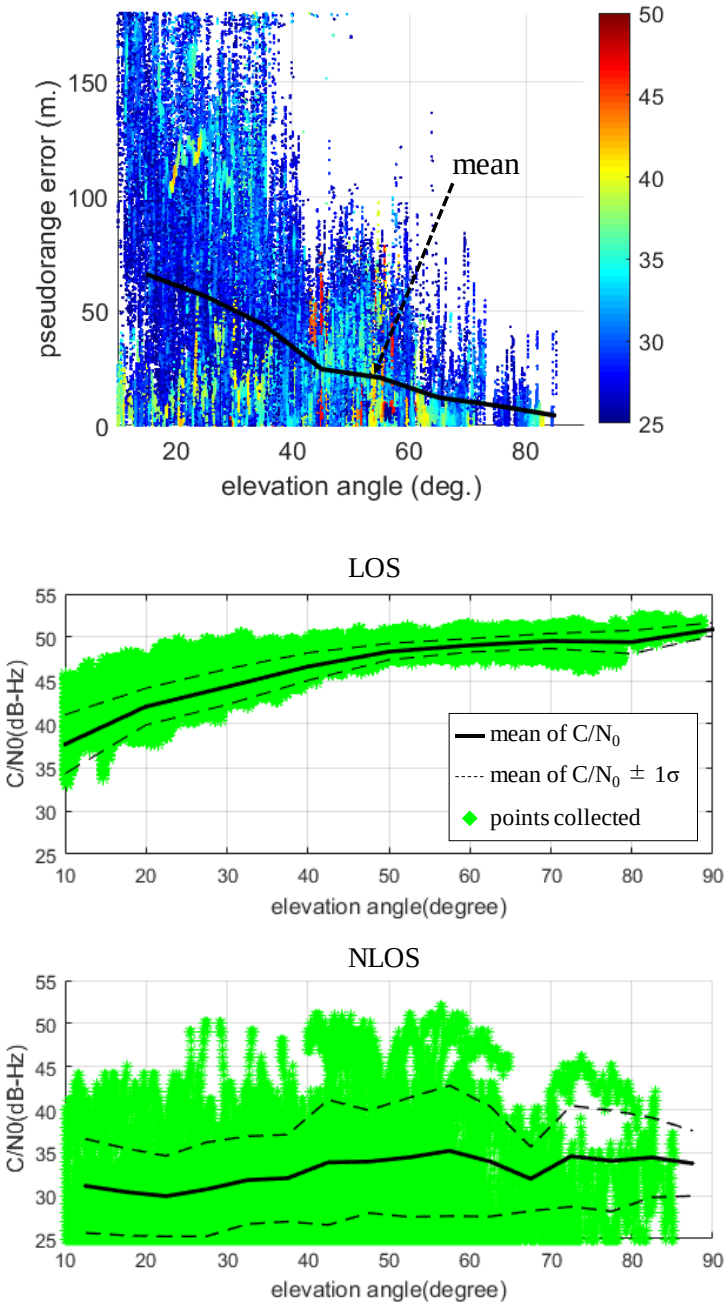

3. OFFLINE PATH PLANNING BASED ON PREDICTED POSITIONING ERROR DISTRIBUTION

The target application of this paper is quart-rotor UAV. It has advantages on flexibility of its movement and easiness to control. In order to ensure its safety to publics, a path planning method that can identify the obstacles (buildings in our application) in the operation area is a minimum requirement. Furthermore, the path planning algorithm should also consider other factors such as shortest path with experiencing minimum GPS positioning error. In general, the flight route of quadcopter is in a fixed altitude which determined by different application. This fixed-height route is able to simplify the mission and movement of quadcopter. In this paper, the process of a quart-rotor flying to the destination from starting point will be planned as following: 1) take-off and climb to an ideal height; 2) fly based on a pre-planned route on the selected height; 3) reach the destination horizontally and landing. For the vertical movement of UAV are usually based on barometer or other sensor rather than GPS. In the other words, the GPS positioning error will not influence UAV in the operation of take-off and landing. Therefore, the path planning will be processed on 2D map with a selected height. The main process of the overall path

planning is shown as Fig.2, *h* represents the operating height. A range of the permitted height for UAV is defined from h_0 to h_{max}. After given the starting take-off point, destination and h_0, the previous predicted positioning error map is used to aid 2D path planning. The path planner will estimate an ideal path for each height until reaching the h_{max}, which is often restricted by governmental law. For example, UAV operation in Hong Kong is limited under about 90 meters. Afterwards, we can compare the performance of the optimal path on each height. Finally, the overall path of the selected height can be obtained and output as our planned ideal path for the UAV operation.

Two different 2D path planning algorithms are introduced in sections 3.1.1 and 3,1,2, respectively. The height selection algorithm is detailed in section 3.2.

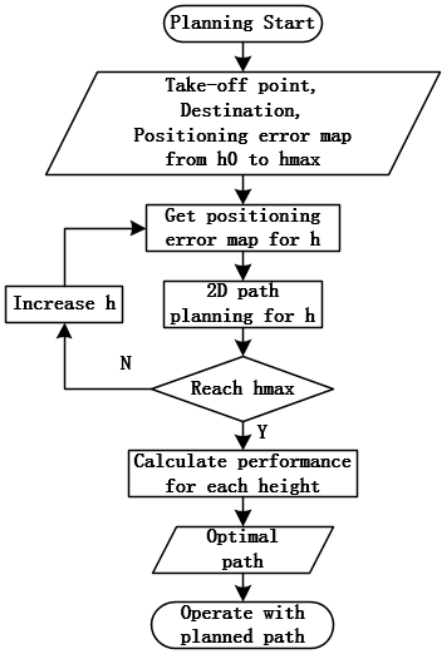

Fig.2 Flow-chart of the 3D path planning for UAV based on positioning error distribution.

3.1.1 2D path planning based on A* algorithm

A* algorithm is a widely-used path planning method to avoid obstacles and reach the destination, also this method is a global scanning method which can solve local optimal problem and select a globally optimal path. The overall process of A* algorithm is shown as Fig.3.

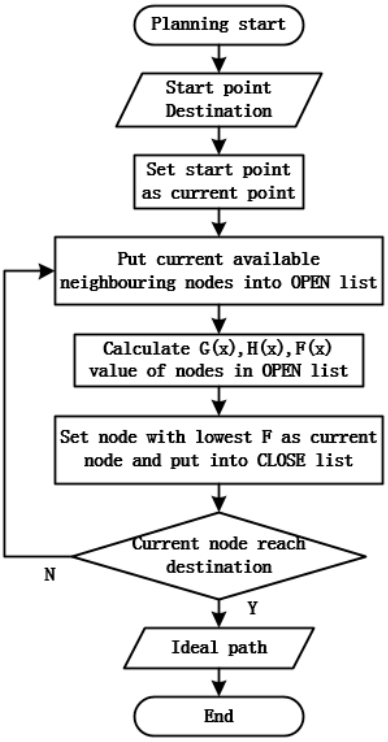

Fig.3 Process of a conventional 2D A* path planning algorithm.

The conventional A* algorithm constructs a group of nodes on the operating map. From the starting node, the A* method identifies whether the neighboring node is available and put all available nodes into an 'open' list. Then, it calculates the cost of all available nodes in the 'open' list assuming as the next step, the calculation is shown as:

$$F(x) = G(x) + H(x) \tag{9}$$

For a specific location *n*, *G(x)* is the minimum traveling distance from starting node to current node and *H(x)* is the minimum distance from current node to the destination node. A* algorithm collects all the available nearby nodes into an open list, the nodes on obstacles will be considered as unavailable nodes. By comparing the overall cost value *F(x)* for the nodes in the 'open' list, the lowest overall cost node will be selected as the next current node and shifted from the 'open' to the 'close' list. By calculating the cost value again and selecting the next step until the current node reach the destination, the 'close' list stores all the selected nodes when reaching to the destination, the ideal path can be obtained via extracting nodes from destination node backwards in the 'close' list.

To improve the conventional A* path planning algorithm in urban area, the positioning error caused by multipath effect should be further considered to avoid quadcopter passing through the GPS hazardous area. With the aid of the predicted positioning error distribution, the positioning error for each node is included into the cost function of A* algorithm. To ensure the safety of UAV in urban area, the major task is to avoid UAV crushing on buildings. Due to multipath effect, the UAV still can contact to buildings by mistakenly recognize its location. To decrease the potential contacts between UAV and building, a variable called the number of contact points N_{ctp} is further defined. It can be introduced by Fig. 4. For a specific location, its predicted positioning error is used as a radius of a circular area, which represents the potential GPS positioning error in that specific location. When the error circle overlaps with a building, it is considered as one contact point. The amount of contact point for a specific location is summed up as N_{ctp}. As shown in Fig.4, the error circle contacts two neighboring buildings as indicated by the red arrow, which represents the N_{ctp} is 2 in this case. The same N_{ctp} calculation can be done for all locations within the simulating area. Thus, a distribution map of N_{ctp} value can be obtained.

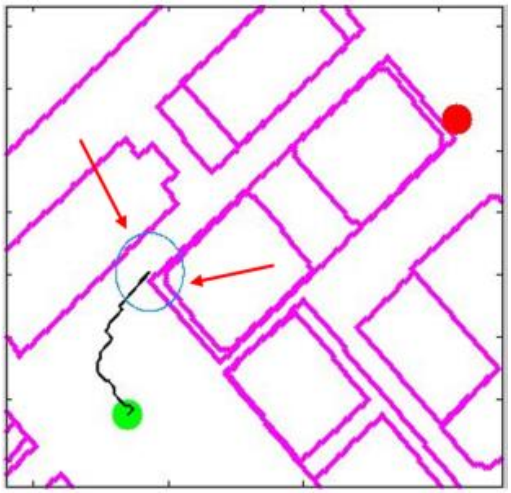

Fig.4 Contact point (red arrow) between buildings and error circle (blue circle) on a specific location (N_{ctp} =2 here).

The contact number is involved into the A* path planning as a part of cost function with a weighting value, the equation of traveling cost difference ΔG and the cost value G for the n[th] node is given as:

$$\Delta G(x) = (1 - k_a) \cdot d_{c-x} + k_a \cdot \mu_a \cdot N_{ctp} \tag{10}$$

$$G(x) = \Delta G(x) + G_p(x) \tag{11}$$

where d_{c-x} is the distance between current node and the next available node, μ_a is a heuristic constant. The amount of contact number can increase the cost value for each approaching available node. Thus, the path with large contact number will be avoided by the proposed A* algorithm. The weighting k_a can balance the proportion between shorter traveling distance and lower contact number, which adapts to different flight requirements. The performance can further adapt to the flight requirements by tuning the weighting value. In this paper, we set k_a as 0.7. Then, the cost value for n[th] node is the summation of the cost value of its parent node $G_p(x)$ and the traveling cost from parent node to current node $\Delta G(x)$. $G(x)$ will be further calculated into overall cost $F(x)$ as equation (9) to determine the idea path with lowest cost. Via the proposed A* path planning algorithm, the ideal 2D path avoiding both obstacles and high positioning area can be planned.

3.1.2 2D path planning based on potential field method

The potential field method constructs a composite artificial potential field in the path planning area. The fields represent the information of target and surrounding obstacles. The destination is defined as an attractive field while the obstacles are defined as repulsive fields. The attractive field creates a force on the object to attract it moving towards the destination. Each repulsive field creates a force to resist the object moving close to the obstacles. The attractive and repulsive force are given as:

$$F_{att}(x) = -k_{att} \left| x - x_g \right| \tag{12}$$

$$F_{rep}(x) = \begin{cases} k_{rep} \left(\frac{1}{x - x_{obs}} - \frac{1}{L_0} \right) \frac{1}{(x - x_{obs})^2} \frac{\partial (x - x_{obs})}{\partial x}, & if \ \ x - x_{obs} \le L_0 \\ 0, \quad if \ \ x - x_{obs} > L_0 \end{cases} \tag{13}$$

where k_{att} is the weighting of attractive force, x is the current location of the UAV, x_g is the location of the goal, k_{rep} is the weighting value of repulsive force, x_{obs} is the location of the obstacle, L_0 is the repulsive force effective range for obstacle. By combining the attractive and repulsive forces, the total force will act on the object to move until the object reaching the destination. Similar to the proposed A* algorithm, the positioning error map should be used in the potential field method. The positioning error map is divided into serial parts. For each part, the locations with positioning error are grouped together. The mean of location of these collected position is defined as the center of the additional potential field. An additional artificial potential field for positioning error is defined as repulsive field to reject the object moving close to high positioning error zone. The repulsive force for positioning error is given as:

$$F_{pe}(x) = \begin{cases} k_{pe}\left(\frac{1}{x-x_{pe}} - \frac{1}{r_{pe}\varepsilon_{pe}}\right)\frac{\varepsilon_{pe}}{(x-x_{pe})^2}, & if\ \ x - x_{pe} \le r_{pe}\varepsilon_{pe} \\ 0, & if\ \ x - x_{pe} > r_{pe}\varepsilon_{pe} \end{cases} \quad (14)$$

k_{pe} representing the weighting of repulsive force from high positioning error area, x_{pe} is the location of the center of additional repulsive field for positioning error, ε_{pe} is the positioning error value of the center of repulsive field and r_{pe} is the heuristic constant of positioning error repulsive field. The value of k_{att}, k_{rep} and k_{pe} are as table.1. The total force on UAV at location X can be calculated as:

$$F_{total}(x) = F_{att}(x) + F_{rep}(x) + F_{pe}(x) \quad (15)$$

The total force $F_{total}(x)$ is used to determine the moving direction and distance of the UAV on next step until it reaching the goal. Finally, the ideal path can be planned with the force effect that helps the UAV to avoid obstacles and hazardous GPS positioning error area.

Table.1 Weighting value for potential field method

variables	k_{att}	k_{rep}	k_{pe}
value	**0.003**	**0.057**	**0.940**

3.2 3D height selection

To select the ideal height for the UAV operation, the proposed 2D A* path planning (or potential field method) will first be applied to each height of the operating area as shown in Fig. 2. Therefore, the optimal 2D path at each height can be obtained. The performance of planned path of each height should be evaluated by both the total travelling distance and total number of potential contact points. We define a performance metric $p(h)$, which is a function of height, to determine which height to operate. Its definition is given as:

$$p(h) = k_p \cdot \mu_p \cdot \bar{N}_{ctp} + (1-k_p) \cdot \frac{d(h)}{d_0} \quad (16)$$

where $d(h)$ is the travelling distance including vertical movement on height h following the planned path, d_0 representing the direct distance between starting point and destination, k_p is 0.7 as the weighting between contact point and travelling distance, μ_p is 3.7 as the balance constant number. We consider the lower $p(h)$ is, the better performance can be obtained. The good performance means the path can avoid crushing on buildings and reduce traveling distance at the same time. Hence, we calculate the $p(h)$ for the planned path at each height, and then select the height with the lowest $p(h)$ as the ideal operating path for UAV. Finally, the optimal path of the selected height and vertical movement for selected height will combine together as the planned 3D path for UAV operation.

4. EXPERIMENT RESULTS AND DISCUSSIONS

4.1 Verification of the prediction of GPS positioning error

To verify the prediction of GPS positioning error, an experiment is conducted to collect real GPS data in the target area. In this study, we use u-blox NEO-M8T GNSS module as Fig.5 to receive raw positioning data. We selected 2 typical locations to collect data for 30 minutes. The receiver is set as 2 meters height to avoid disturbance from pedestrian. The experiment and predicted positioning result are shown in Figs. 6 and 7, respectively. The comparison between the real (experimental) and predicted GPS positioning error is listed in Table 2. The intersection is in a relative open area. As shown in Fig. 6, the experiment result shows the positioning error is smaller comparing to that in the narrow canyon. The left of Fig. 7 shows, the predicted error is very similar to the real positioning error. The narrow canyon is surrounded by high buildings, which resulted in larger positioning error comparing to intersection one. The predicted error in narrow canyon in also large, which is corresponding to the experiment result. The experiment device could be disturbed by other factors such as foliage, but the prediction only consider the multipath effect. Thus, it is reasonable that the experiment error may larger than prediction. In

general, the overall tendency of positioning error is similar between prediction and experiment. As a result, the predicted GPS error is verified to adapt with most cases to model the positioning error distribution.

Fig.5 U-blox NEO M8T GNSS module with antenna

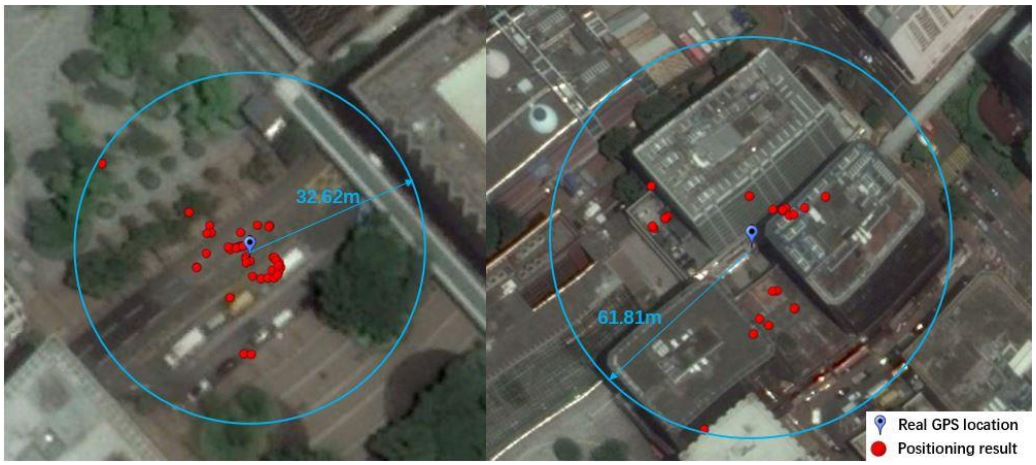

Fig.6 Experimental GPS positioning result for 30 minutes. Left and right panels show the results in the intersection and the narrow canyon, respectively. Red spots for positioning result, blue balloon for real GPS location.

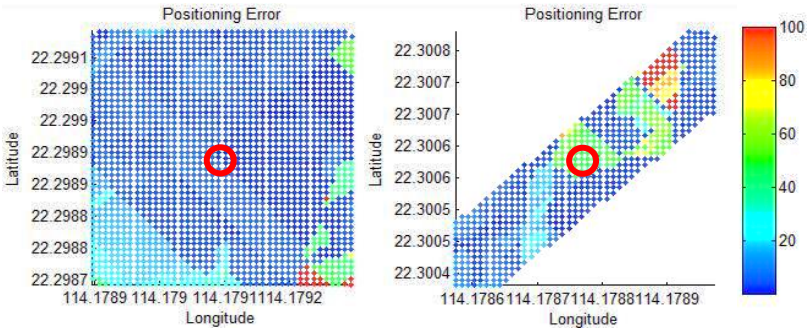

Fig.7 Predicted positioning error for the experiment location. Left and right panels show the results in the intersection and the narrow canyon, respectively. The color bar denotes the positioning error in meters.

Table.2 Comparison between experimental and predicted GPS positioning error

	Experiment		Simulation
	Mean positioning error (m)	Max positioning error (m)	Mean positioning error (m)
Intersection	6.38	32.62	5.25
Narrow canyon	24.68	61.81	42.33

4.2 Processing the predicted positioning error map

For the proposed UAV path planning algorithm, the 2D positioning error maps at different height are required as shown in Fig.8. As height increases, the overall positioning error is reduced. This is due to the lessen multipath effect and the increase of direct signal on higher altitude. When the height is over 50 meters, the predicted error for most area is reduced to almost zero since most buildings are built within 50 meters height. We select two points to better demonstrate the drop of GPS positioning error as shown as Fig.9. In the case of open field (blue line), the multipath signal ratio is increased at the height of 25 meter and keep dropping when height increasing. the positioning error also follows this tendency. In the case of near building point, the positioning error is large on the ground. It starts to drop after 22 meters in height. The error slightly increases between 37 and 47 meters in height due the increase of ratio of multipath and total signal ratio. When the height is increasing, the positioning error may increase at some situations. It is due to the receiver receives more NLOS signal at lower altitude. Thus, the ratio of multipath signal is increased, resulting larger error. Thus, the multipath error cannot always consider as decreasing when the height is increasing. An ideal flight height may not always the rules of the higher the better. This paper uses path planning performance to select the ideal height for operation.

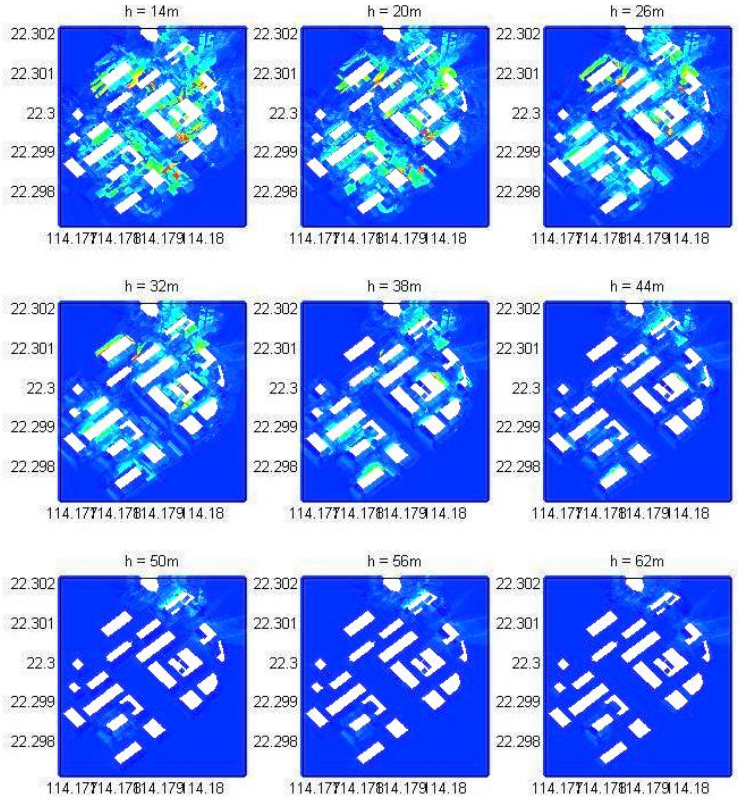

Fig.8 2D GPS positioning error map at heights between 14 to 62 meters. The resolution is 6 meters for each layer.

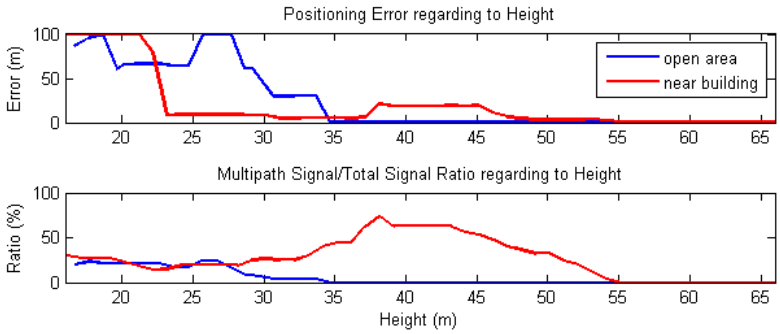

Fig.9 Selected points to demonstrate the change of positioning error associated by height change. Blue and red lines indicate the result of locations in open area and nearby buildings, respectively.

4.3 Evaluation of the proposed 2D path planning methods.

There are four algorithms compared, and they are:

1. Conventional A* algorithm – using building information as obstacle,
2. Proposed A* algorithm – using both building information and the predicted GPS positioning error,
3. Conventional potential field method – using building information, and
4. Proposed potential field method – using both building information and the predicted GPS positioning error.

To apply the proposed path planning algorithm, the positioning error map is predicted for the operation area as shown in Fig.10. The path planning result of the conventional A* algorithm is shown as Fig.10. The flight route starts from the star node to the cross node as the dash line. Without considering the GPS positioning error in path planning, the route is planned directly to destination avoiding buildings. UAV follows the planned route may fly through hazardous zone, such as red or yellow zone in Fig.10. The red and yellow zones represent the area that GPS error exceed 60 meters. UAV may mistakenly detect its location and fly towards the obstacles causing air crush if flying through these areas. For the proposed A* algorithm, the path planning result is presented as the chain line in Fig.10. The UAV can identify the high positioning error area and avoid passing through it. The planned path may experience a longer travelling distance but it significantly reduces the experienced positioning error in its path. The comparison between the conventional and proposed A* algorithms is shown in Fig.11. The number of contact point and positioning error of the proposed A* algorithm is significantly decreased comparing with that of the conventional A*. In brief, the proposed A* algorithm is able to plan a path with less multipath effect, which means traveling on a safer path for UAV operation in urban area.

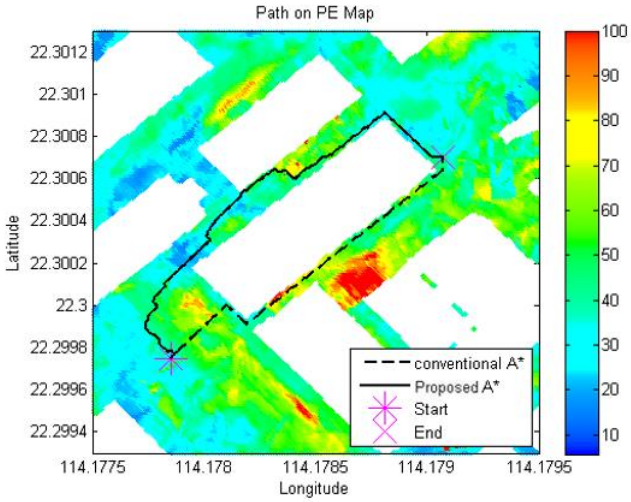

Fig.10 Conventional and proposed A* path planning algorithm based on positioning error map. Obstacles (buildings) are constructed as white area. The color bar denotes the positioning error in meters.

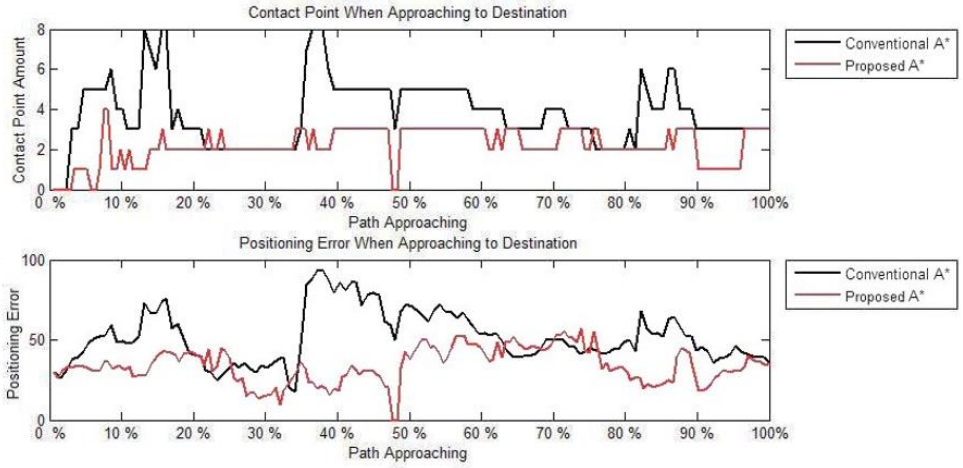

Fig.11 Contact point amount and positioning error comparison between the conventional and the proposed A* algorithms. X-axis denotes the percentage of route finished.

The results of conventional (consider only building) and the proposed (consider both building and GPS error) potential field methods are shown in left and right panels of Fig.12, respectively. Their experienced positioning errors when approaching to destination are shown in Fig.13.

The conventional potential field method straightly travels through the narrow gap between buildings. However, the proposed potential field method considers the positioning error distribution on its path. It has the tendency to avoid the area with large GPS error. Thus, its experienced positioning error is slightly less than that of the conventional method. However, the proposed potential field method still suffers from the local optimal problem. It will always go through the narrow gap, then even through it takes the positioning error map into consideration. Its overall performance does not have great improvement comparing with the conventional method.

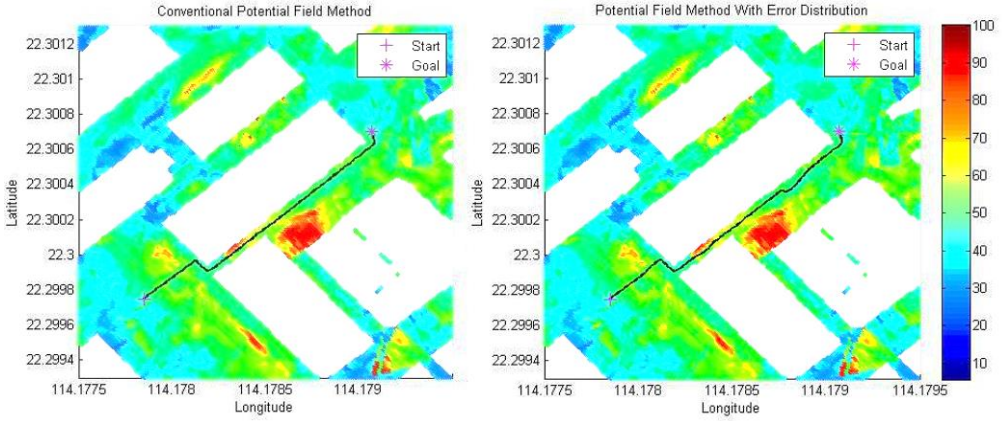

Fig.12 Path planning result for conventional potential field method (left) and improved potential field method (right). The color bar denotes the positioning error in meters.

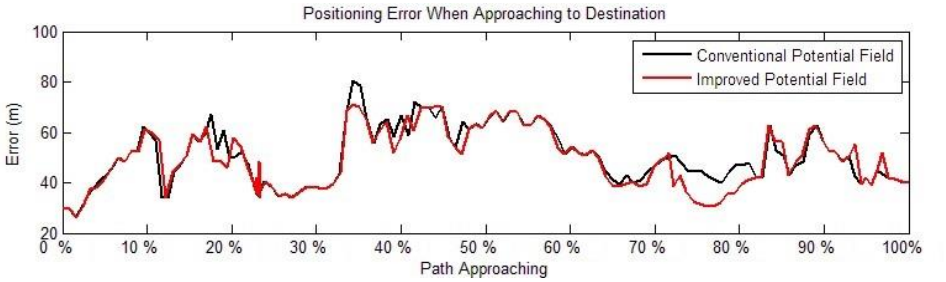

Fig.13 Positioning error approaching to destination for potential field method. X-axis denotes the percentage of route finished. Black line denotes conventional potential field method; red line denotes improved potential field method.

Their performance of each algorithm is listed in Table.3. 1.1 Comparison between different path planning algorithms

Table.3 Performance comparison between different path planning algorithm

	Traveling distance (m)	Mean positioning error (m)	Mean contacting point amount
A*	**183.64**	**51.92**	**3.79**
Proposed A*	**241.41**	**33.95**	**2.18**
Potential field	**164.10**	**49.91**	**3.29**
Proposed potential field	**166.26**	**48.75**	**3.21**

The potential field methods have better performance than the A* algorithm in terms of travelling distance. For the point of view of safety operation, the proposed A* algorithm design a route that experienced less GPS positioning error. It results in the potential contacting points to buildings (probability of crash) is also lower comparing to other methods. However, the proposed method requires longer travelling distance to reach the destination. For improved potential field method, it planned path could avoid some of the erroneous positioning area such as red area in Fig. 12. In addition, its computational load is lower than the A* algorithms. However, due to the previous mentioned problem of local minimum, its designed path could still encounter the area with high probability of crash. The potential field method has limitations. including 1) the local optimal problem; 2) existing trapping area. The trapping area means the path planning fails to reach the destination and stuck in the midway. This

phenomenon is usually occurred in complex geometry of buildings. Based on the reasons above, we concluded that the proposed A* algorithm is preferred to process the off-line path planning for UAV in urban area.

4.4 Evaluation of 3D path planning result

The 3D path planning means to select a height layer with the best 2D planning as introduced in Fig. 2. The conventional and proposed A* algorithms are evaluated in this subsection. A typical UAV urban transporting scenario, UAV starts from a ground location and travels to another ground destination, is tested. The results of the 2D path at different height are listed in Table.4.

Table.4 Performance of the 2D path at different height layer.

Conventional A*										
Height (m)	15	25	35	40	45	50	60	70	**80**	90
Traveling distance(m)	124.62	138.33	158.33	168.33	173.47	183.47	203.47	223.47	**243.47**	263.47
Mean of experienced positioning error (m)	17.29	12.54	8.36	5.55	5.05	3.98	3.93	3.79	**3.57**	3.37
Mean of contact number	1.073	0.921	0.461	0.427	0.360	0.348	0.348	0.326	**0.281**	0.281
p(h)	3.300	2.927	1.729	1.667	1.498	1.497	1.557	1.555	**1.492**	1.552
Proposed A*										
Height (m)	15	25	35	40	**45**	50	60	70	80	90
Traveling distance(m)	363.37	241.97	197.53	201.43	**210.68**	224.43	241.75	259.69	267.17	282.53
Mean of experienced positioning error (m)	6.98	7.70	3.43	4.45	**3.64**	3.08	3.04	2.91	2.41	2.01
Mean of contact number	0	0.106	0.062	0.026	**0**	0	0	0	0	0
p(h)	1.082	1.009	0.757	0.671	**0.627**	0.668	0.720	0.773	0.796	0.841

To observed Table.4, the experienced positioning error and potential contact number are decreased as the height increased. Namely, the risk is smaller when UAV flies higher. Note that the positioning error during the vertical movement can be neglected because barometer is usually implemented for the estimation of UAV flying altitude. On the other hand, the travelling distance is increased while the height increased because the vertical travelling distance is also considered. By applying the defined performance metric *p(h)*, the compromise between travelling distance (cost) and potential contact number (risk) can be done. The minimum *p(h)* of the conventional A* is 1.492, which is occurred in the layer of 80 meters in height. The proposed A* achieves 0.627 of the minimum *p(h)*, which is occurred in 45 meters height. Thus, the path planned by the proposed A* is not only travelled less distance but also safer. The planned 2D paths at 80 and 45 meters are shown in the left and right panels of Fig.14. In Fig. 14, if the height of building is higher than the selected height of planed path, the building will be plotted as white one. Conversely, the building is lower than the selected height will be plotted as transparent one. As shown in Fig. 14, there is a high building on the right side of the planned route. This building reflects GPS signals, resulting in about 20 meters of multipath error in the vicinity of it. The path planned by the proposed method intelligently avoid the area. This capability is important especially in flying UAV in urban area. It can reduce the risk for the UAV operation.

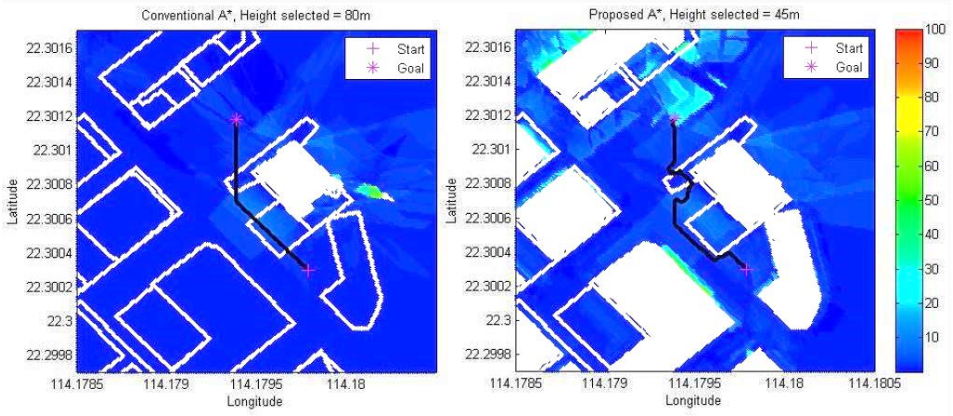

Fig.14 Overall planned path for ground (22.3003º, 114.1798) to ground (22.3012º, 114.1794) travelling scenario in urban area. Left and right panels demonstrate the conventional A* method and the proposed A* method respectively.

Three additional typical UAV urban transporting scenarios tested for the 3D path planning, and they are: A1) starts from a ground location and travels to the roof of a building; A2) starts from the roof of a building and travels to a ground destination; A3) starts from the roof of a building and travels to another roof of a building. The results can be found in Appendix. By comparing the results on different scenarios, the proposed A* path planning algorithm is able to design a path with lower experienced GPS error at lower or same height. Namely, a route with lower risk for UAV operation. However, in some scenarios, the proposed path requires extra travel distance comparing with the conventional one.

5. CONCLUSIONS

In this study, the multipath effect of GPS positioning in the urban area is modelled and predicted via the 3D building model, ray-tracing simulation and broadcast almanac. By the use of it, the GPS positioning result can be predicted. The prediction is verified by comparing it with the real GPS positioning error at an intersection and narrow canyon in the urban area of Kowloon, Hong Kong. In the verification, the real and predicted positioning error have the similar level and tendency. This paper proposes a new A* path planning algorithm considering both the maps of obstacle and potential GPS positioning error. According to the experiment result, the proposed algorithm is able to determine an ideal path to avoid positioning hazardous area. Thus, it is more preferable for safety of the operation comparing with other path planning algorithms such as conventional A* and potential field methods. In the UAV mission, we suggest that the quadcopter first take-offs vertically to a certain height. Then, it flies horizontally to the 2D position of the destination. Finally, it lands vertically to the destination. Based on this idea, a new 3D path planning method is developed using the result of the 2D A* algorithm. Four typical UAV transporting scenarios are tested. Comparing the results of conventional and proposed 3D A* algorithms, the latter one achieves higher safety on lower height. In the other words, the proposed A* path planning more than the conventional one.

However, the presented method still has the following drawbacks: 1) high computation loads for GPS error prediction that required to be pre-processed before the flight; 2) the planned path may have sharp turning angle which introduced energy lost for quadrotor. Other UAV platform might not be valid to use the proposed path planning due to the sharp turning; 3) The proposed method is an offline path planning. The online path planning is still required to adjust the change of the environment. Regarding to the drawbacks, the future work is to improve trajectory smoothness in the path planning algorithm and integrate sensors for dynamic detection.

REFERENCES

1. Erdelj, M. and E. Natalizio. *UAV-assisted disaster management: Applications and open issues*. in *2016 International Conference on Computing, Networking and Communications (ICNC)*. 2016.
2. Caibing, X. and B. Shaofeng. *Research on BeiDou positioning performance in urban environments*. in *2013 IEEE International Conference on Signal Processing, Communication and Computing (ICSPCC 2013)*. 2013.
3. Christian, E., K. Lasse, and K. Heiner, *Real-Time Single-Frequency GPS/MEMS-IMU Attitude Determination of Lightweight UAVs.* Sensors, 2015. **15**(10): p. 26212-26235.
4. Birk, A., et al., *Safety, Security, and Rescue Missions with an Unmanned Aerial Vehicle (UAV).* Journal of Intelligent & Robotic Systems, 2011. **64**(1): p. 57-76.
5. Song, Y., et al., *Towards autonomous control of quadrotor unmanned aerial vehicles in a GPS-denied urban area via laser ranger finder.* Optik - International Journal for Light and Electron Optics, 2015. **126**(23): p. 3877-3882.
6. Leishman, R., T. McLain, and R. Beard, *Relative Navigation Approach for Vision-Based Aerial GPS-Denied Navigation.* Journal of Intelligent & Robotic Systems, 2014. **74**(1): p. 97-111.
7. Zhu, H., H. Xin, and C. Zheng, *Research On UAV Path Planning.* Applied Mechanics and Materials, 2011. **58-60**: p. 2351.
8. Medeiros, F. and J. Silva, *Computational Modeling for Automatic Path Planning Based on Evaluations of the Effects of Impacts of UAVs on the Ground.* Journal of Intelligent & Robotic Systems, 2011. **61**(1): p. 181-202.
9. Moon, S., E. Oh, and D. Shim, *An Integral Framework of Task Assignment and Path Planning for Multiple Unmanned Aerial Vehicles in Dynamic Environments.* Journal of Intelligent & Robotic Systems, 2013. **70**(1): p. 303-313.
10. Dong, Z., et al. *A hybrid approach of virtual force and A* search algorithm for UAV path re-planning*. in *2011 6th IEEE Conference on Industrial Electronics and Applications*. 2011.
11. Khuswendi, T., H. Hindersah, and W. Adiprawita. *UAV path planning using potential field and modified receding horizon A* 3D algorithm*. in *Proceedings of the 2011 International Conference on Electrical Engineering and Informatics*. 2011.
12. Lin, C.L., et al. *Flight path planning for mini rotor UAVs*. in *11th IEEE International Conference on Control & Automation (ICCA)*. 2014.

13. Meister, O., et al. *Adaptive path planning for a VTOL-UAV*. in *2008 IEEE/ION Position, Location and Navigation Symposium*. 2008.
14. Kong, Z. and B. Mettler, *Evaluation of Guidance Performance in Urban Terrains for Different UAV Types and Performance Criteria Using Spatial CTG Maps.* Journal of Intelligent & Robotic Systems, 2011. **61**(1): p. 135-156.
15. Xia, L., et al. *Path planning for UAV based on improved heuristic A* algorithm*. in *2009 9th International Conference on Electronic Measurement & Instruments*. 2009.
16. Hawa, M., *Light-assisted A* path planning.* Engineering Applications of Artificial Intelligence, 2013. **26**(2): p. 888-898.
17. Filippis, L., G. Guglieri, and F. Quagliotti, *Path Planning Strategies for UAVS in 3D Environments.* Journal of Intelligent & Robotic Systems, 2012. **65**(1): p. 247-264.
18. Garcia, M., A. Viguria, and A. Ollero, *Dynamic Graph-Search Algorithm for Global Path Planning in Presence of Hazardous Weather.* Journal of Intelligent & Robotic Systems, 2013. **69**(1): p. 285-295.
19. Sun, X., C. Cai, and X. Shen, *A New Cloud Model Based Human-Machine Cooperative Path Planning Method.* Journal of Intelligent & Robotic Systems, 2015. **79**(1): p. 3-19.
20. Zhan, W., et al., *Efficient UAV Path Planning with Multiconstraints in a 3D Large Battlefield Environment.* Mathematical Problems in Engineering, 2014. **2014**.
21. Tseng, F.H., et al. *A Star Search Algorithm for Civil UAV Path Planning with 3G Communication*. in *2014 Tenth International Conference on Intelligent Information Hiding and Multimedia Signal Processing*. 2014.
22. Krawiec, B., K. Kochersberger, and D. Conner, *Autonomous Aerial Radio Repeating Using an A*-Based Path Planning Approach.* Journal of Intelligent & Robotic Systems, 2014. **74**(3): p. 769-789.
23. Chen, X. and J. Zhang. *The Three-Dimension Path Planning of UAV Based on Improved Artificial Potential Field in Dynamic Environment*. in *2013 5th International Conference on Intelligent Human-Machine Systems and Cybernetics*. 2013.
24. Montiel, O., R. Sepúlveda, and U. Orozco-Rosas, *Optimal Path Planning Generation for Mobile Robots using Parallel Evolutionary Artificial Potential Field.* Journal of Intelligent & Robotic Systems, 2015. **79**(2): p. 237-257.
25. Mac, T.T., et al. *Improved potential field method for unknown obstacle avoidance using UAV in indoor environment*. in *2016 IEEE 14th International Symposium on Applied Machine Intelligence and Informatics (SAMI)*. 2016.
26. Allaire, F., et al., *FPGA Implementation of Genetic Algorithm for UAV Real-Time Path Planning.* Journal of Intelligent and Robotic Systems, 2009. **54**(1): p. 495-510.
27. Zhang, B., et al., *Geometric Reinforcement Learning for Path Planning of UAVs.* Journal of Intelligent & Robotic Systems, 2015. **77**(2): p. 391-409.
28. Vanegas, F. and F. Gonzalez, *Enabling UAV Navigation with Sensor and Environmental Uncertainty in Cluttered and GPS-Denied Environments.* Sensors, 2016. **16**(5): p. 666-666.
29. Frontera, G., et al., *Approximate 3D Euclidean Shortest Paths for Unmanned Aircraft in Urban Environments.* Journal of Intelligent & Robotic Systems, 2016.
30. De Filippis, L., G. Guglieri, and F. Quagliotti, *A Minimum Risk Approach for Path Planning of UAVs.* Journal of Intelligent & Robotic Systems, 2011. **61**(1): p. 203-219.
31. Hsu, L.-T., Y. Gu, and S. Kamijo, *3D building model-based pedestrian positioning method using GPS/GLONASS/QZSS and its reliability calculation.* The Journal of Global Navigation Satellite Systems, 2016. **20**(3): p. 413-428.
32. Dierendonck, A.J., P. Fenton, and T. Ford, *Theory and Performance of Narrow Correlator Spacing in a GPS Receiver.* Navigation, 1992. **39**(3): p. 265-283.
33. Garin, L., F. van Diggelen, and J.-M. Rousseau. *Strobe and edge correlator multipath mitigation for code*. in *ION GPS-96*. 1996.

Appendix – 3D path planning results in the three additional scenarios

The scenario A1 for UAV travelling from a specific location on the ground (22.2996,114.1780) to the roof of a building (22.2996,114.1772). The selected height layer is 55m and 40m by the conventional and proposed A* algorithms, respectively.

Table.5 Path performance regarding to height for scenario A1

Conventional A*									
Height (m)	25	35	40	45	**50**	60	70	80	90
Traveling distance(m)	111.76	131.76	141.76	151.76	**161.76**	178.87	198.87	218.87	238.87
Mean positioning error (m)	10.96	4.01	2.46	1.41	**0.96**	1.01	1.01	1.01	1.01
Mean contact number	0.814	0.326	0.209	0.093	**0.012**	0.023	0.023	0.023	0.023

p(h)	2.465	1.264	0.994	0.725	**0.546**	0.631	0.695	0.759	0.822
proposed A*									
Height (m)	25	35	**40**	45	50	60	70	80	90
Traveling distance(m)	223.92	184.36	**150.43**	154.65	162.72	180.80	200.80	220.80	240.80
Mean positioning error (m)	7.10	3.46	**1.98**	1.20	0.96	1.01	1.01	1.01	1.01
Mean contact number	0.145	0.034	**0**	0	0	0	0	0	0
p(h)	1.089	0.676	**0.480**	0.493	0.519	0.577	0.641	0.705	0.768

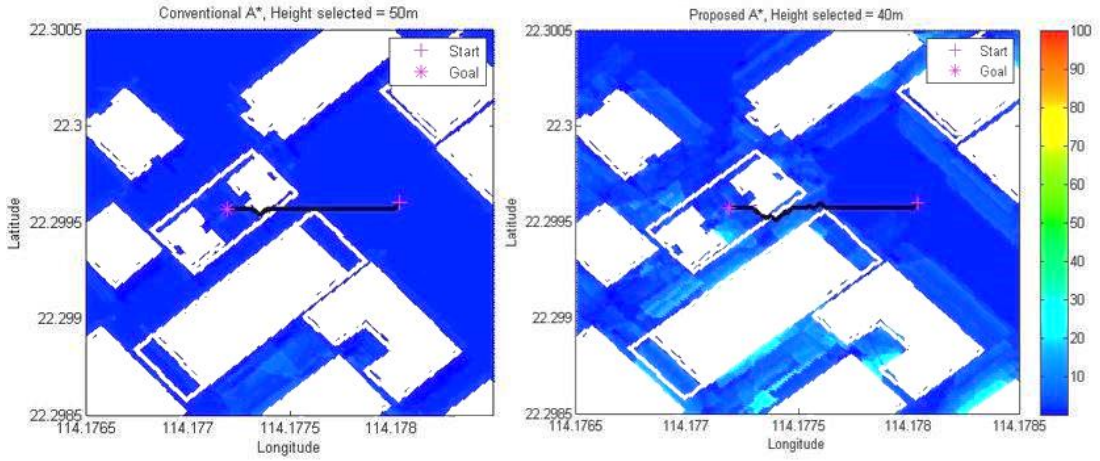

Fig.15 Path planning trajectory for scenario A1. White frame contours represent the building below the selected height, and white solid building is the higher than the selected height.

The scenario A2 for UAV travelling from the roof of a building (22.2983,114.1783) to a specific location on the ground (22.2983,114.1773). The selected height layer is 55m and 45m by the conventional and proposed A* algorithms, respectively.

Table.6 Path performance regarding to height for scenario A2

Conventional A*									
Height (m)	25	35	40	45	50	60	**70**	80	90
Traveling distance(m)	121.37	141.37	151.37	161.37	171.37	191.37	**211.37**	229.44	249.44
Mean positioning error (m)	9.95	8.99	4.91	3.23	2.77	1.84	**1.03**	1.01	1.01
Mean contact number	0.387	0.484	0.183	0.161	0.140	0.075	**0.032**	0.043	0.043
p(h)	1.359	1.668	0.918	0.891	0.865	0.757	**0.704**	0.785	0.843
Proposed A*									
Height (m)	25	35	40	**45**	50	60	70	80	90
Traveling distance(m)	133.55	156.44	171.54	**172.93**	176.18	199.98	217.09	231.37	251.37
Mean positioning error (m)	7.22	7.20	3.55	**3.29**	2.74	1.65	1.15	1.01	1.01
Mean contact number	0.085	0.064	0.010	**0**	0	0.010	0	0	0
p(h)	0.612	0.624	0.530	**0.507**	0.517	0.614	0.637	0.679	0.738

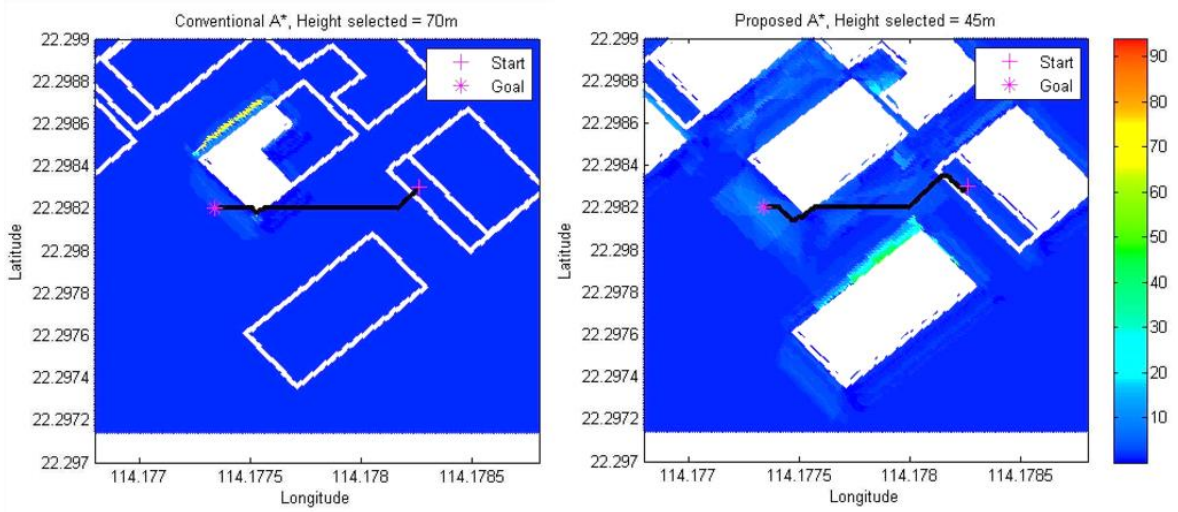

Fig.16 Path planning trajectory for scenario A3. White frame contours represent the building below the selected height, and white solid building is the higher than the selected height.

The scenario A3 for UAV travelling from the roof of a building (22.3006,114.1796) to the roof of another building (22.3010,114.1776). Both the conventional and proposed A* algorithm select the layer of 55 meters' height.

Table.7 Path performance regarding to height for scenario A3

Conventional A*								
Height (m)	30	40	50	**55**	60	70	80	90
Traveling distance(m)	268.61	288.16	308.61	**302.24**	312.24	332.24	352.24	372.24
Mean positioning error (m)	7.86	7.67	2.03	**1.84**	1.84	1.80	1.80	1.80
Mean contact number	0.480	0.617	0.179	**0.128**	0.128	0.128	0.128	0.122
p(h)	1.608	1.992	0.882	**0.742**	0.755	0.782	0.810	0.824
Proposed A*								
Height (m)	30	40	50	**55**	60	70	80	90
Traveling distance(m)	413.23	341.47	340.65	**329.18**	339.18	357.59	375.67	399.03
Mean positioning error (m)	4.90	2.97	1.66	**1.42**	1.42	1.337	1.323	1.281
Mean contact number	0.011	0.004	0.004	**0**	0	0	0	0
p(h)	0.589	0.476	0.475	**0.448**	0.462	0.487	0.511	0.543

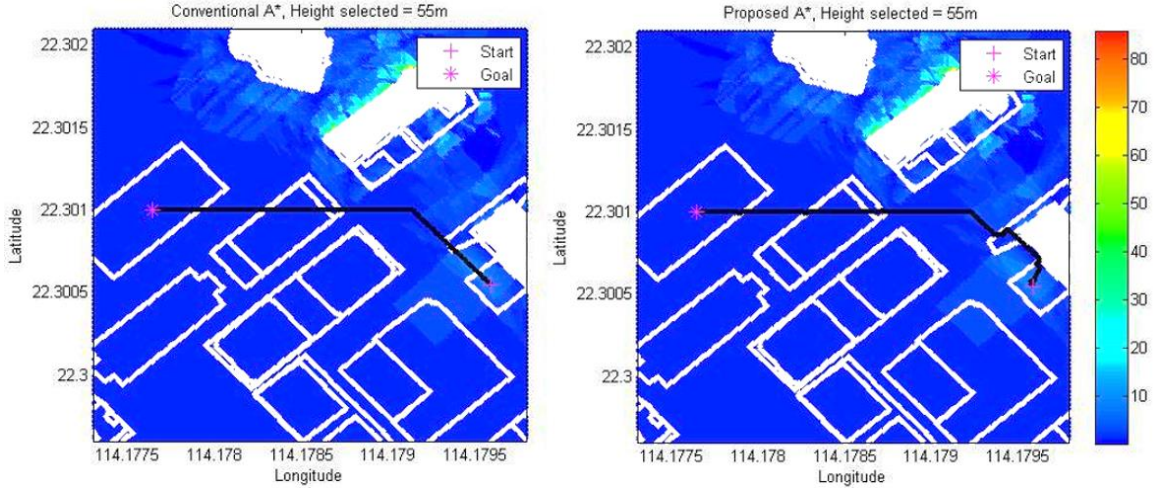

Fig.17 Path planning trajectory for scenario A3. White frame contours represent the building below the selected height, and white solid building is the higher than the selected height.